Journal of Colloid and Interface Science 677 (2025) 250–263

Contents lists available at ScienceDirect

Journal of Colloid And Interface Science

journal homepage: www.elsevier.com/locate/jcis

Regular Article

Colloid, interface, and foam properties of water-soluble polyglycerol esters solutions

Rumyana D. Stanimirova [a,*], Krassimir D. Danov [a], Mihail T. Georgiev [a], Jordan T. Petkov [a,b,c]

[a] Department of Chemical & Pharmaceutical Engineering, Faculty of Chemistry & Pharmacy, Sofia University, 1164 Sofia, Bulgaria
[b] Arxada, Hexagon Tower, Crumpsall Vale, Blackley, Greater Manchester, M9 8GQ, UK
[c] Biological Physics, School of Physics and Astronomy, The University of Manchester, Schuster Building, Oxford Road, M13 9PL, UK

GRAPHICAL ABSTRACT

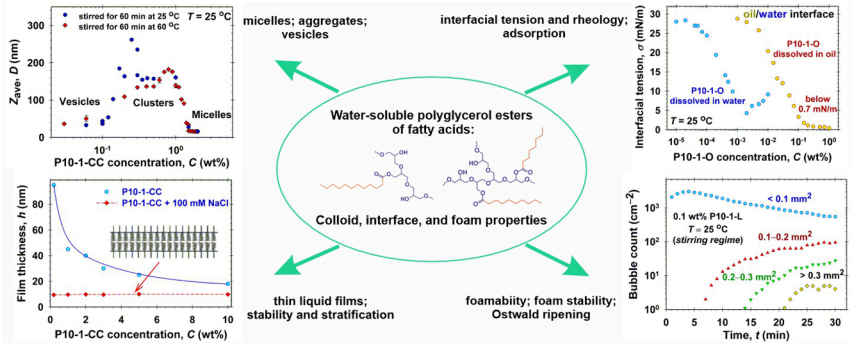

ARTICLE INFO

Keywords:
Water-soluble polyglycerol esters of fatty acids
Static and dynamic interfacial properties
Bulk aggregation and micellization
Thin liquid films stability and stratification
foaming and Ostwald ripening

ABSTRACT

Hypothesis: Polyglycerol esters of fatty acids are generated via the esterification of a polydisperse mixture of polyglycerol with naturally derived fatty acids. The polymerization process of polyglycerol results in the production of various oligomers, ranging from di-, tri-, and higher-order forms, which contribute to the complexity of final products. The combination of complementary experimental techniques and adequate theoretical interpretations can reveal the wide variety of their physicochemical properties.

Experiments: The colloid and interface properties of polyglyceryl mono-laurate, mono-stearate, mono-oleate, and a mixture of mono-caprylate and mono-caprate esters solutions were characterized by measurements of the electrolytic conductivity, static and dynamic surface tension, aggregate and micelle sizes and distributions, thin liquid film stability and stratification, and solubility in aqueous and in oil phases. The formation, stability, and bubble size distribution of foams generated from polyglycerol esters aqueous solutions were systematically investigated.

Findings: The low concentrations of double-tail molecules and fatty acids in polyglycerol esters affect considerably their micellar, aggregation, and vesicle formations in aqueous solutions. The theoretical data interpretation of polyglycerol esters isotherms and thin liquid films data provide information on the adsorption energies, excluded areas per molecule, interaction parameters of molecules at interfaces, surface electrostatic potential, and the size of micelles. Polyglyceryl mono-oleate exhibits spontaneous emulsification properties. Short chain

* Corresponding author.
E-mail address: rs@lcpe.uni-sofia.bg (R.D. Stanimirova).

https://doi.org/10.1016/j.jcis.2024.07.219
Received 23 May 2024; Received in revised form 19 July 2024; Accepted 27 July 2024
Available online 29 July 2024

length polyglycerol esters have excellent foaming ability but relatively low foam stability. The optimal weight fractions of the short-chain polyglyceryl esters and polyglyceryl mono-stearate mixtures with respect to good foaminess and foam stability upon Ostwald ripening are obtained. The reported physicochemical characterization of the water-soluble polyglycerol esters could be of interest to increase the range of their applicability in practice.

1. Introduction

Polyglycerol esters are nonionic surfactants composed of a mixture of glycerol polymers esterified with fatty acids or interesterified with triglycerides [1–7]. Short and long fatty acid polyglycerol esters have been also enzymatically synthesized using Lippozime 435 as a catalyst in solvent-free systems [8]. The esters of oligo-(glycerol carbonate-glycerol) are new biobased oligomeric surfactants with an excellent ability to stabilize inverse and multiple emulsions [9]. The sulfosuccinic derivatives of fatty polyglycerol esters [10] are characterized by the cosmetological compatibility of renewable raw materials. Depending on the degree of glycerol polymerization and the fatty acid chain lengths, their physicochemical properties may vary considerably: low and high molecular weight; water or oil soluble; solid or liquid; mono-, di- or polycarboxylic single or mixed acid esters; mono-, di- or polyesters of the polyglycerol; HLB values in the range from 4 to 13.

Polyglycerol esters (PGE) are biodegradable, biocompatible, non-carcinogenic and non-toxic. They do not cause adverse effects even at a test concentration of 5 wt% and fulfill the requirements of safety, bio-based economy, and sustainable development [4–6,11]. PGE are widely used: in the food industry [1,3,12–16]; cosmetics, pharmacy, and medicine [6,17–22]; in the oil industry [23]; as emulsifiers for monodisperse emulsions in the membrane emulsification processes [24,25]; etc. This type of nonionic surfactants is suitable for the production of: water-in-oil-in-water double emulsions, which have applications as vehicles for encapsulation and delivery of nutrients during food digestion or for drug release [26–30]; nano-, mini-, and fast inverted emulsions [31–35]; core-multishell nanocarriers, nanodispersions, and vesicles [36–40]. The foamability and foam stability of polyglycerol esters solutions are studied in the literature [41–44]. In Ref. [45], the authors reported that diglyceryl mono-myristate dissolved in different nonaqueous solvents can be used for producing super stable nonaqueous foams. After the pioneering work of Curchellas et al. [43], the scanning force microscope became a tool to investigate the skins of foam bubbles and to get information on the aggregation adsorption of PGEs at air–-water interfaces.

Because of the challenges associated with the structural complexity of polyglycerol esters, only few studies have addressed their colloid and interface properties. The surface tension isotherms of polyglyceryl mono-laurate and mono-caprylates show that the critical micelle concentration (CMC) increases and the adsorption at the CMC decreases with an increase in the number of glycerol units in the molecules [9,32,38,46–48]. The effects of additives on the adsorption of polyglycerol esters are examined in Ref. [49] and the impact of the number of fatty acid residues on the phase behavior of decaglycerol fatty acid esters is studied in Ref. [50]. One convenient way to characterize the structure-interfacial properties relationship and to quantify the amphiphilicity of polyglycerol esters is the Phase-Inversion-Temperature-slope method [51].

Our goal in the present study is to characterize the colloid, interface, and foam properties of commercially available polyglyceryl mono-laurate, mono-stearate, mono-oleate, and a mixture of mono-caprylate and mono-caprate esters solutions without additional purification. The combination of complementary experimental techniques (electrolytic conductivity, dynamic and static light scattering, surface and interfacial tension isotherms and dilatational rheology measurements, thin liquid films stability and stratification, dynamic surface tension, foamability, foam stability, and bubble size distributions) provides adequate information on the physicochemical properties of the studied PGEs. The materials and used experimental methods are presented in Section 2. The colloid and interface properties, aggregation, adsorption and interfacial characteristics are reported in Section 3. Section 4 includes information on the thin liquid films and stratification of micellar polyglycerol esters solutions. The correlation between dynamic surface tension and adsorption with the foamability, foam stability, and Ostwald ripening is considered in Section 5. The general conclusions are summarized in Section 6.

2. Materials and methods

2.1. Materials

We studied a range of water-soluble polyglycerol esters of fatty acids characterized by diverse chain lengths provided by Arxada. They are generated via the esterification of a polydisperse mixture of polyglycerol with naturally derived fatty acids. The polymerization process of polyglycerol results in the production of various oligomers, ranging from di-, tri-, and higher-order forms (Fig. 1 and Fig. S1), which contribute to the complexity of the final products. The comparative analysis of the weight fractions of linear versus branched oligomers is shown in Fig. 1a. The molecular weight of the resulting polyglycerol esters is calculated considering the polyglycerol oligomer distribution and the respective fatty acid. The specific polyglycerol esters included in this study are as follows. Geomulse^{TM} C15 RSPO MB, termed below as P10-1-CC, is roughly an equimolar mixture of polyglyceryl mono-caprylate and polyglyceryl mono-caprate with average molecular weight M_w = 454.3 g/mol. Geomulse^{TM} L15 RSPO MB (P10-1-L) is polyglyceryl mono-laurate ester (Fig. 1b), M_w = 496.9 g/mol; Geomulse^{TM} S10 RSPO MB Pastille (P10-1-S) is polyglyceryl mono-stearate ester, M_w = 580.3 g/mol; Geomulse^{TM} O13 RSPO MB (P10-1-O) is polyglyceryl mono-oleate ester, M_w = 578.6 g/mol.

The electrolytic conductivity measurements reveal that the samples might contain minuscule concentrations of indifferent electrolytes (Fig. S2), which are insufficient to influence the interfacial and micellar properties of the surfactant solutions. All examined products contain traces of fatty acids and dual-hydrocarbon-tailed polyglycerol esters (cf. Fig. 1c), which affect considerably the interfacial and colloid properties of the studied surfactants (see *Sec.* 3). The natural pH of all polyglycerol ester solutions is maintained consistently around 6.1 ± 0.2, signifying their chemical stability and broad application potential. All samples have been used as received.

2.2. Solution preparation

The aqueous solutions were prepared using deionized water via Elix 3 water purification system (Millipore, USA) with a specific resistivity of 15 MΩ·cm. All experiments were carried out at temperature of 25 °C. P10-1-S and P10-1-O required one hour of stirring and heating at 60 °C to achieve complete dissolution. P10-1-O is partially soluble in both aqueous and oily phases and exhibits spontaneous emulsification properties in the presence of oily phases (Fig. S3). P10-1-CC and P10-1-L show good solubility at room temperature – the respective solutions are transparent for concentrations lower than 0.3 wt% and turbid for higher surfactant concentrations (see *Sec.* 3.1 and Fig. S4). To check the effect of stirring and temperature on the aggregate size distribution, the respective P10-1-CC and P10-1-L solutions were stirred for one hour at

60 °C and cooled down to 25 °C.

We used specific additives to investigate the nature of the intermolecular interactions and phase behavior: i) Urea (Sigma Aldrich, Cat. No. U1250) inhibited the hydrogen bond formation among polyglycerol headgroups; ii) $ZnCl_2$ (Sigma Aldrich, Cat. No. 793523) was used to study the impact of trace fatty acids on the interfacial rheology; iii) NaCl (Sigma Aldrich, Cat. No. 7647145) was employed to control the electrostatic interactions in the thin film experiments; iv) NaOH (Sigma Aldrich, Cat. No. S5881) and HCl (Sigma Aldrich, Cat. No. 258148) – to adjust the pH.

The interfacial tension measurements and the phase exchange studies at oil/solution interfaces were conducted using sunflower oil (SFO, commercial grade) and light mineral oil (LMO, Sigma Aldrich Cat. No. M5904, a mixture of C15-C40 alkanes from mineral sources). The SFO was purified by passing through a chromatography column filled with Silica Gel and Florisil as adsorbents. The measured interfacial tension against water was typical for pure SFO (31 mN/m) with less than a 0.2 mN/m decreasing over 60 min.

2.3. Experimental methods and protocols

Static and dynamic surface tension. The static surface tension at air/solution interface was measured by the Du Noüy ring method on force tensiometer K100 (Krüss, Germany) equipped with a platinum–iridium ring. In the case of oil/water interfaces, the interfacial tension was studied using the pendant drop method on DSA 100R (Krüss GmbH, Germany). The implemented software fits the experimental pendant drop profile with the Laplace equation of capillarity and calculates the surface tension, drop volume and area.

For diffusion-controlled adsorption, the equilibrium surface tension, σ_{eq}, is estimated from the well-known relationship:

$$\sigma(t) = \sigma_{eq} + \frac{a}{\sqrt{t}} \quad (1)$$

where $\sigma(t)$ is the value of the surface tension at time t and a is a constant, which depends on the experimental conditions. The surface tension relaxations of P10-1-CC and P10-1-L solutions show that the adsorption processes are diffusion-controlled (Fig. 2a). In these cases, Eq. (1) was applied to obtain the most probable values of σ_{eq} and to construct the surface tension isotherms. In contrast, the surface tension relaxations of P10-1-S solutions are very slow (Fig. 2b), the adsorption process is barrier-controlled, and the formed adsorbed layers are viscoelastic and insoluble. The solid lines in Fig. 2b correspond to the exponential decay fits of $\sigma(t)$ vs t. For example, the dependence of the surface tension of 3.0 $\times 10^{-4}$ wt% P10-1-S solution on time is practically a linear function for $t < 1800$ s. It decreases from 61 mN/m to 58 mN/m for 30 min (Fig. 2b), so that σ_{eq} is not possible to be determined correctly. For the same concentration of P10-1-CC, the equilibrium surface tension is well measurable and $\sigma_{eq} = 39.7 \pm 0.1$ mN/m (Fig. 2a).

The dynamic surface tension of polyglycerol esters solutions was measured using the maximum bubble pressure method on BP 100 automated bubble pressure tensiometer (Krüss GmbH, Germany) [52].

Phase exchange experiments. Phase exchange experiments [53] were carried out to determine the surface or interfacial tensions using axisymmetric drop shape analysis on DSA100R instrument (Krüss GmbH, Germany), employing U-shaped capillaries (Fig. S5). The oscillating bubble (drop) method was applied to calculate the surface dilatational storage, E', and loss, E'', moduli. The bubble (drop) surface area, $A(t)$, oscillates with a relatively low amplitude and period of oscillations 5 s, the respective oscillations of $\sigma(t)$ are measured to calculate E' and E''. The exchange of aqueous phase was realized by a cartridge pump, which simultaneously supplies pure water and sucks out the old aqueous solution from the working cuvette keeping the fluid volume constant.

The typical experimental protocol is the following [53]. A bubble (drop) is formed in each polyglycerol ester solution and the relaxation of the surface tension to a steady state value, close to σ_{eq}, is measured. During the first experimental stage, one performs oscillatory surface deformations to measure the surface dilatational moduli E' and E'' corresponding to a given value of $\sigma(t)$. For example, three surface oscillatory deformations (O1, O2, and O3) are performed through the first

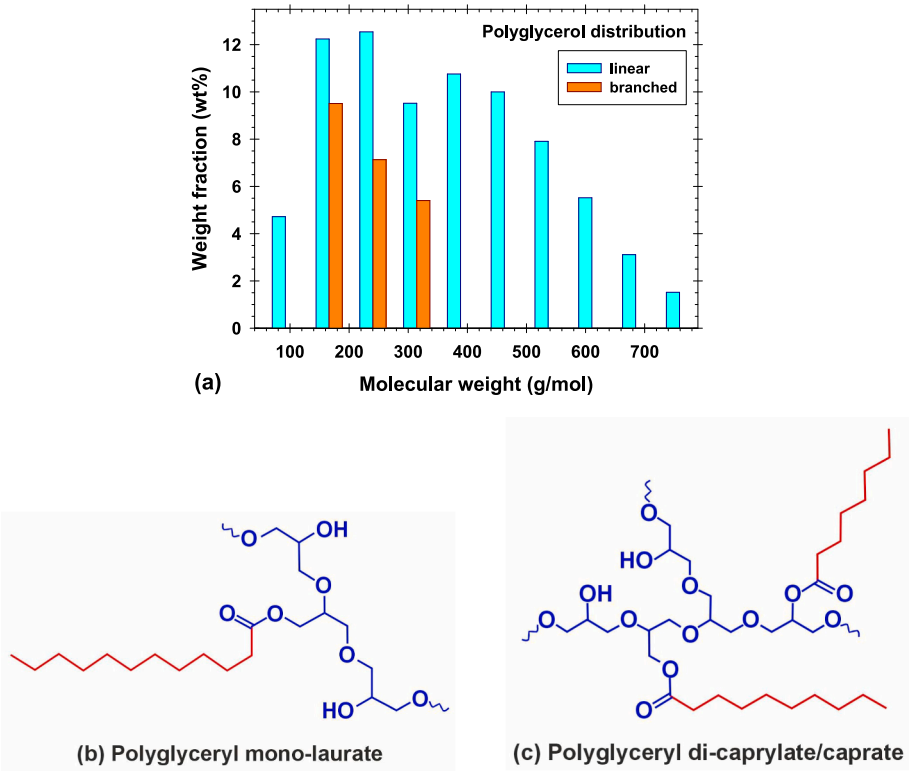

Fig. 1. Weight distribution of polyglycerol (a). Chemical structure of polyglycerol esters: b) polyglyceryl mono-laurate; c) polyglyceryl di-caprylate/caprate.

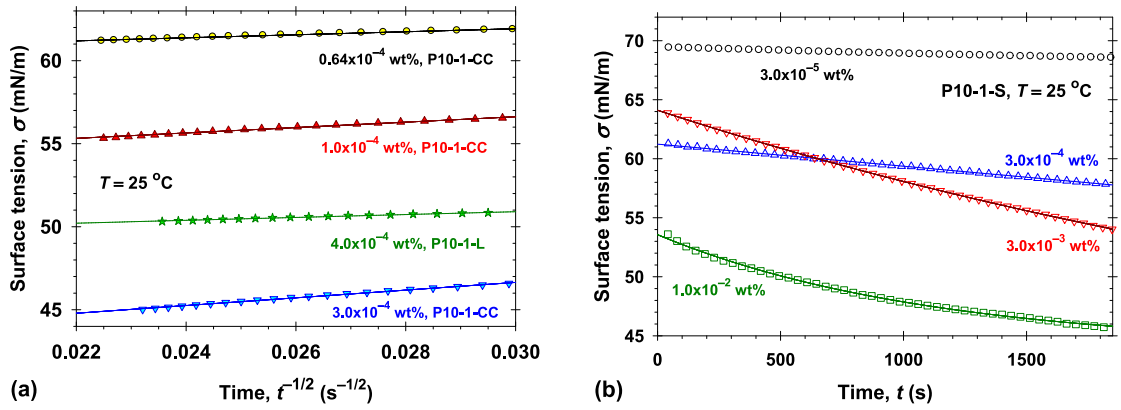

Fig. 2. Typical surface tension relaxation data for polyglycerol esters: a) $\sigma(t)$ vs one over square root of time, $t^{-1/2}$, for P10-1-CC and P10-1-L solutions; b) $\sigma(t)$ vs time, t, for P10-1-S solutions.

stage in Fig. S6. In the second experimental stage, the surfactant solution is exchanged with pure water (PhE1) to rinse the bubble's (drop's) adsorption layer. As expected upon the removal/washing of polyglycerol esters, the surface tension increases and oscillatory experiments (O4 and O5 in Fig. S6) are performed to measure the interfacial rheology and to quantify the effect of polyglycerol esters desorption and the potential presence of less water-soluble adsorbed molecules (if any), which were not washed from the respective interface. To ensure the complete replacement of the surfactant solution with pure water and to maximize the washing, the phase exchange procedure (PhE1) and subsequent surface oscillatory deformations are repeated two or three times (PhE2, PhE3 in Fig. S6).

Dynamic (DLS) and static (SLS) light scattering. The size distributions of the aggregates (micelles and/or vesicles) in polyglycerol esters solutions were analyzed using Malvern 4700C light scattering system (Malvern Instruments, UK). This apparatus combines the dynamic and static light scattering capabilities, enabling a detailed assessment of the aggregate sizes. Equipped with a goniometric arrangement, the system allows angle-dependent measurements, essential for the Zimm plot analysis. The SLS measurements were conducted at various of concentrations and angles, θ, and processed with the classical Zimm equation: $Kc/R(\theta) = 1/M_w + 2A_2c + \ldots$, where K is the optical constant, c is the concentration, $R(\theta)$ is the excess Rayleigh ratio at angle θ, M_w is the weight-average molecular weight, and A_2 is the second virial coefficient.

The dynamic light scattering (DLS) was used to determine the hydrodynamic diameter of aggregates with measurements conducted at a fixed angle of $\theta = 90°$. This angle was chosen to optimize the sensitivity and accuracy of the hydrodynamic diameter calculations. All measurements (both DLS and SLS) were performed at a controlled temperature of 25 °C.

Thin liquid films. The Scheludko-Exerowa (SE) capillary cell [54] was utilized to study the drainage, stratification, equilibrium and critical thicknesses of thin foam films stabilized with polyglycerol esters solutions. The studied solution is loaded into a cylindrical capillary through a small opening in the wall. Subsequently, the solution is drawn out from the capillary resulting into a biconcave drop, the two menisci approach each other until a liquid film is formed in the central part of the cell. The size of the formed foam film is adjusted by injecting or sucking liquid through the orifice. The radii of thin foam films illustrated in Fig. 7 and Figs. S13–S15 are in the range from 600 μm to 700 μm. The interferometric method is used to measure the film thickness, h, vs time t. The capillary cell is kept closed to eliminate evaporation – in this case, the driving force for the film thinning is the capillary pressure. After reaching of the steady-state equilibrium thickness for infinitely stable films, the capillary cell is opened to the atmosphere, which leads to an evaporation from the film surfaces, that causes a considerable increase of the pressure difference, thus ending into the formation of a molecular bilayer film or eventually to a film rupture.

Foaming, foam stability, and bubble size distribution. The formation, stability, and bubble size distribution of foams [55] were investigated by using Dynamic Foam Analyzer DFA100 (Krüss, Germany). This device has a high-resolution camera, allowing for precise measurements of bubble size distributions and detailed foam characterization. For the comprehensive characterization of the foam properties, we applied two working regimes (Fig. S7). For the illustration of the bubble size distribution in Tables S4–S6, the micrographs of respective foams are taken in the frame of 6 mm width by 5 mm height. In the sparging (bubbling) regime, the foam is generated by bubbling of gas through a glass porous frit in the surfactant solutions. The technical parameters for this process are finely tuned to ensure reproducibility and accuracy: 0.4 dm^3/min or 0.8 dm^3/min flow rates; 50 ml surfactant solution; 100 mm height position of the camera to capture detailed foam structure images. In the stirring regime, the foam is alternatively produced by mechanical agitation using a standard propeller (SR4501, Kruss). The conditions for this regime were carefully selected based on preliminary trials to optimize the reproducibility of obtained results: 30 s duration for foam formation; 6000 rpm stirring speed; 10 s oscillation period of propeller; 50 ml working surfactant solution; 55 mm height position of the camera to capture the dynamics and structure the studied foam.

3. Solubility, turbidity, interfacial tension isotherms, and interfacial rheology

3.1. Solubility and turbidity

Geomulse^{TM} C15 RSPO MB exhibits excellent water solubility at room temperature, with solutions remaining clear at concentrations both below 0.3 wt% and above 2 wt% (Fig. S4a). To check the effect of stirring temperature on the solution turbidity, the P10-1-CC solutions were stirred at 60 °C for one hour and subsequently cooled down to 25 °C. The absorbance data vs concentration (Fig. S4b) suggest that the temperature variations have minimal influence on the turbidity, with the highest absorbance observed at a concentration of 0.8 wt%. The results from DLS and SLS experiments with P10-1-CC solutions at different surfactant concentrations, C, are summarized in Fig. 3a and Fig. S8, respectively. We observed two concentration ranges with a relatively low polydispersity (Fig. S8a): i) vesicles with an average diameter of 45 nm for $C<0.15$ wt%; ii) for $C>1.5$ wt%, the predominant structures are micelles with a mean size of 15 nm. The presence of vesicles at lower concentrations is attributed to the double-tail polyglycerol esters molecules, which, upon increasing concentration, are solubilized by the single-tail polyglycerol esters micelles, leading to the predominance of smaller 15 nm micelles. For P10-1-CC concentrations 0.15 wt% $< C<$1.5 wt%, large aggregates with a well pronounced

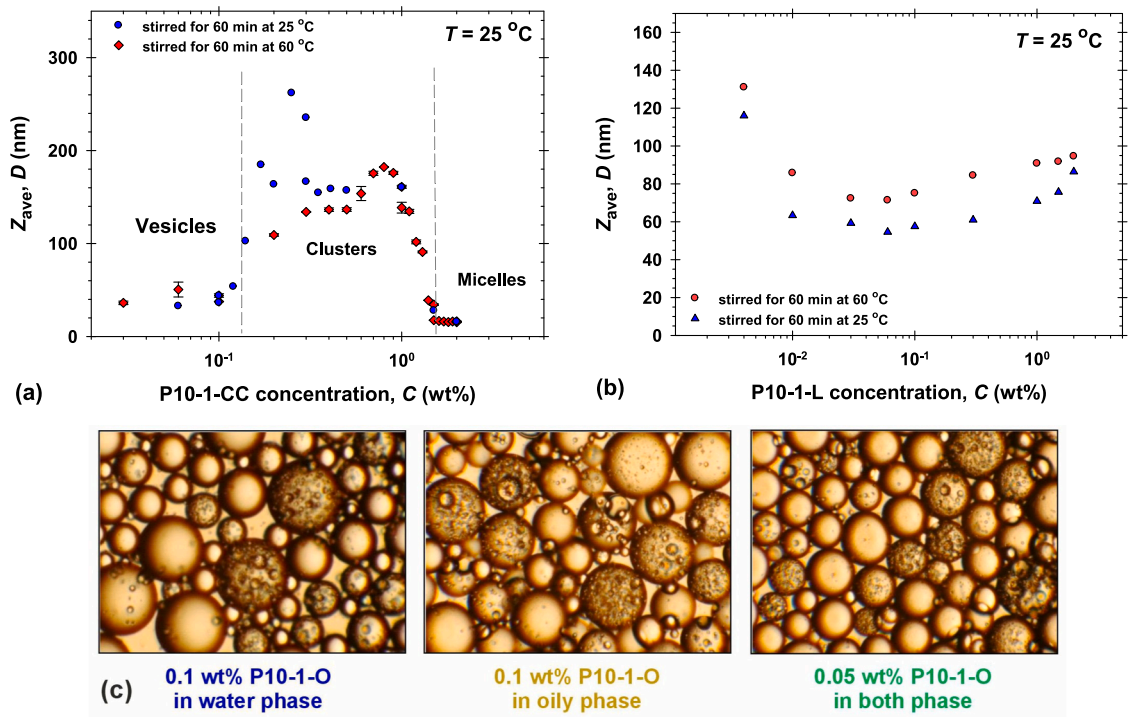

Fig. 3. Dependence of the average sizes of polyglycerol esters on the surfactant concentration obtained from DLS experiments: a) P10-1-CC; b) P10-1-L. c) Microscopic images of 0.1 wt% P10-1-O stabilized emulsions when P10-1-O is dissolved in the different phases.

polydispersity are formed (Fig. S8a). Applying the Zimm plot approach for the SLS measurements (Fig. S8b), one obtains an average mass of 96153 g/mol per aggregate, which corresponds to an assembly of approximately 212 P10-1-CC molecules. The downward slope of the Zimm plot line indicates an attractive interaction between the aggregates. One possible explanation could be that all single-tail monomers preferentially form micelles, while the available double-tail molecules have the tendency to form vesicular structures. Once the number of single-tail esters reaches a threshold concentration, the double-tail esters are solubilized in the micelles.

In the case of P10-1-L, the mean aggregate sizes are approximately independent on surfactant concentration *C*, and on the temperature of solution preparation. The average aggregate diameter is around 80 nm with low polydispersity and the solution turbidity increases monotonically with concentration *C*, see Fig. S8c. The mole fraction of the double-tail monomers in P10-1-L sample is more than 200 times lower than that in P10-1-CC (see Section 3.2). As it is expected, the turbidities of P10-1-S solutions are higher than those of P10-1-CC and P10-1-L solutions due to their longer hydrocarbon tails and propensity for aggregation (Fig. S8c).

As noted in Section 2, P10-1-O is soluble in both water and oily phases. If one dissolves P10-1-O in water and subsequently layers SFO on top without mixing, then one observes intensive mass transfer of the P10-1-O molecules from the aqueous solution to the oil (Fig. S3). Due to a significant drop in the interfacial tension as a result of the adsorption of P10-1-O, a spontaneous emulsification takes place – water droplets appear in the oily phase and oily droplets in the aqueous phase, respectively. To highlight the P10-1-O unique emulsification properties, we prepared emulsions by using a 50:50 blend of water and SFO phases. The total P10-1-O surfactant concentration was 0.1 wt%. The surfactant was dissolved either only in the aqueous phase, only in the oily phase, or in the both phases 0.05 wt% in water and 0.05 wt% in oil. Fig. 3c shows microscopic images of these emulsions. Surprisingly, in all cases we observed stable oil in water emulsions. According to the classical Bancroft rule, P10-1-O should form water in oil emulsions because it is more soluble in the oily phase (see Section 3.2).

3.2. Interfacial tension isotherms

The used polyglycerol esters samples might contain a minute amount of oil-soluble surface-active components. To evaluate their adsorption capability at interfaces, we agitated 10 mL purified SFO+30 mL 0.1 wt% polyglycerol esters aqueous solutions to prepare coarse emulsions. These emulsions were then maintained at a constant temperature of 25 °C for 24 h in a thermostat to ensure complete saturation of the oil droplets. The saturated SFO phases were separated by destroying the emulsions by centrifugation. Subsequently, the interfacial tension of the saturated oil/pure water interface vs time was measured (Fig. 4a). The measurements revealed a notable reduction in the interfacial tensions for all polyglycerol esters: 25 mN/m for P10-1-S; 20 mN/m for P10-1-L; 14 mN/m for P10-1-CC. This indicates that P10-1-CC contains the highest concentration of oil-soluble admixtures, while P10-1-S has the lowest.

The interfacial tension isotherms of P10-1-O solutions are shown in Fig. 4b in both cases of: P10-1-O dissolved in water (aqueous solution/purified SFO interface); P10-1-O dissolved in SFO (pure water/SFO solution interface). From the slopes of the interfacial tension vs ln*C* close to the kink points of the isotherms, one estimates approximately equal values of the saturation adsorption, $\Gamma_{sat} = 2.81 \pm 0.07$ μmol/m^2, and the area per adsorbed molecule of 0.59 ± 0.01 nm^2. As it should be in this case, the established equilibrium adsorption layer is independent on the phases in which P10-1-O is initially dissolved. However, the concentrations corresponding to equal values of the interfacial tensions differ significantly, being two orders of magnitude lower for P10-1-O dissolved in water. This underlines the P10-1-O higher solubility in the oily phase and results in a notably reduced minimal interfacial tension (below 0.7 mN/m) when P10-1-O is initially dissolved in SFO.

The experimental surface tension isotherms of P10-1-CC and P10-1-L aqueous solutions are summarized in Fig. 4c and Fig. 4d, respectively. It is well illustrated that the kink points of isotherms are at 0.001 wt% for P10-1-CC and at 0.003 wt% for P10-1-L. In the literature, the authors reported higher value of 0.003 wt% for P10-1-CC [32]. For purified di-, tri-, tetra-, and pentaglycerol monolaurates, the measured CMC values are 0.105 mM, 0.187 mM, 0.283 mM, and 0.295 mM, respectively [47].

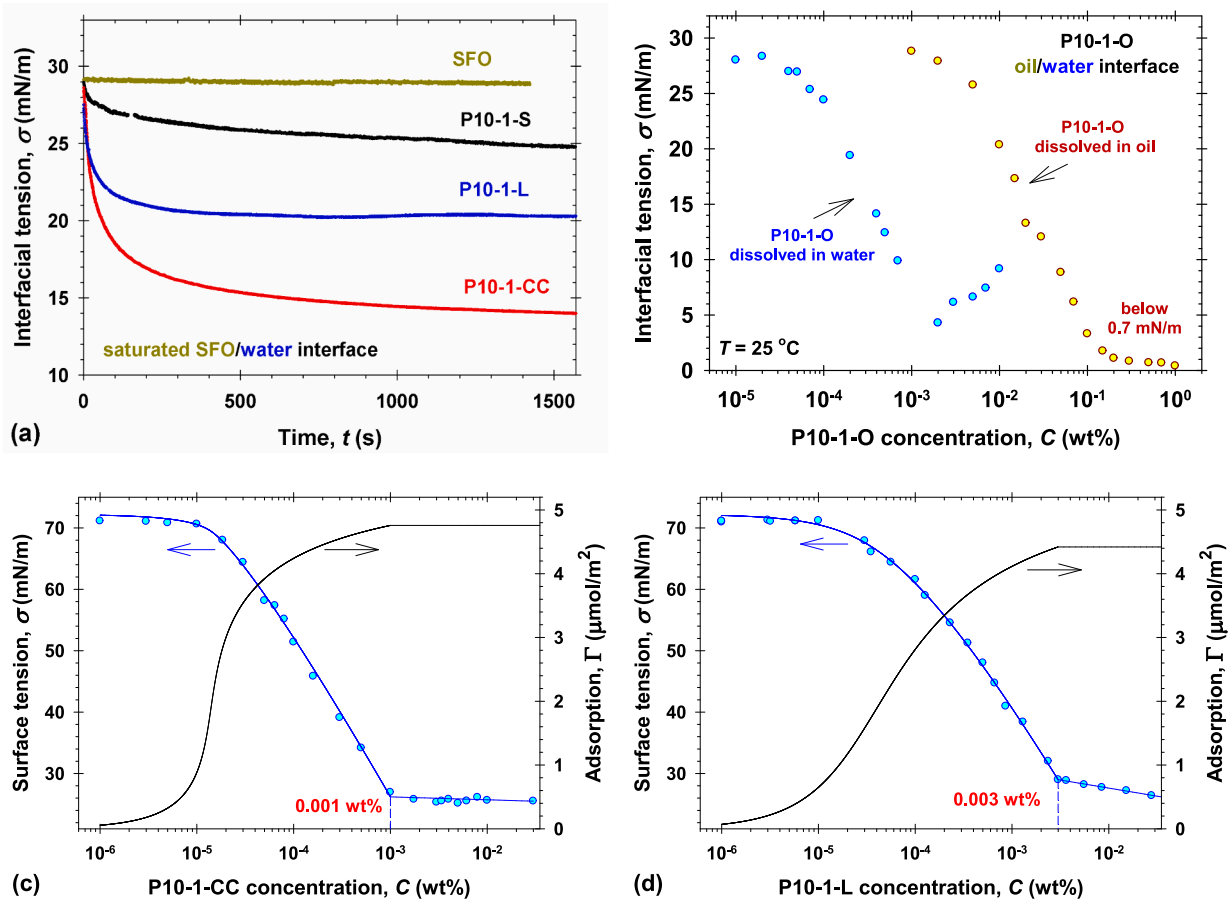

Fig. 4. a) Surface tension of saturated oil/water interface vs time. b) Oil/water interfacial tension vs p10-1-o concentration. Surface tension isotherms and adsorptions of: c) p10-1-cc aqueous solutions; d) p10-1-l aqueous solutions.

These concentrations are considerably higher than 0.06 mM (0.003 wt %) given in Fig. 4d. Thus, the obtained experimental kink point concentrations (Fig. 4c and Fig. 4d) correspond to the critical aggregate bulk concentrations (CAC), see Section 3.1. The unexpected fact that the CAC for P10-1-CC is lower than that for P10-1-L needs an additional explanation because the length of the hydrocarbon tails of P10-1-CC is shorter than that of P10-1-L.

The experimental surface tension isotherms of polyglycerol esters aqueous solutions in Fig. 4c and Fig. 4d are processed using the van der Waals type of adsorption model [56,57]:

$$KC = \frac{\Gamma\alpha}{1-\Gamma\alpha}\exp\left(\frac{\Gamma\alpha}{1-\Gamma\alpha} - \beta\Gamma\alpha\right) \quad (2)$$

Here: k_B is the Boltzmann constant; Γ is the adsorption; K is the equilibrium adsorption constant; α is the minimal (or "excluded") area per molecule; β is the dimensionless interaction parameter, which is positive for attraction between the adsorbed molecules in lateral direction. The respective expression for the two-dimensional equation of state corresponding to the van der Waals model reads:

$$\sigma = \sigma_0 - k_B T\frac{\Gamma}{1-\Gamma\alpha} + k_B T\beta\frac{\Gamma^2\alpha}{2} \quad (3)$$

where $\sigma_0 = 72.2$ mN/m is the surface tension of pure water at 25 °C. The adsorption constant K, is directly related to the free energy of adsorption, E_{exp}, and to the molar volume of the adsorbed species, ν_m, by the following relationship:

$$K = \nu_m\exp\left(\frac{E_{exp}}{k_B T}\right) \quad (4)$$

The solid lines in Fig. 4c and Fig. 4d show the best theoretical fit results using Eqs. (2) and (3) and three adjustable parameters: K; α; β. The excellent description of experimental data is achieved with: $1/K$=2.34 μM, $\alpha = 0.29$ nm^2, $\beta = 5.50$ for P10-1-CC; $1/K$=1.63 μM, $\alpha = 0.29$ nm^2, $\beta = 1.52$ for P10-1-L. The values of the saturation adsorptions are 4.76 μmol/m^2 for P10-1-CC and 4.42 μmol/m^2 for P10-1-L.

The obtained values of the excluded area per molecules are equal and reasonable. From adsorption constants and Eq. (4), one calculates the adsorption energies: $1/\nu_m = 2.42$ M and $E_{exp} = 13.8\,k_B T$ for P10-1-CC; $1/\nu_m = 2.21$ M and $E_{exp} = 14.1\,k_B T$ for P10-1-L. From the well-accepted Tanford rule [58], one estimates that the adsorption energy of P10-1-CC should be E=9.43 $k_B T \ll E_{exp}$ and that of P10-1-L – E=12.2 $k_B T < E_{exp}$. These considerable differences confirm that the PGE samples contain admixtures of double-tail molecules (Fig. 1c). The energy of adsorption of double-tail molecules is expected to be $2E$ (one sees that $E < E_{exp} < 2E$) and their molar volume – to be $2\nu_m$. Thus, the adsorption constant, K, becomes equal to:

$$K = (1-x)\nu_m\exp\left(\frac{E}{k_B T}\right) + 2x\nu_m\exp\left(\frac{2E}{k_B T}\right) \quad (5)$$

where x is the mole fraction of the double-tail species. As a result, we estimated that P10-1-CC sample contains 0.31 mol% double-tail molecules and P10-1-L sample contains more than 200 times lower number of double-tail molecules, 0.0014 mol%. This fact explains the vesicle formation in the case of P10-1-CC and the absence of vesicles in the case of P10-1-L, see Section 3.1.

The experimental interfacial tension isotherms (SFO/aqueous surfactant solution) for water soluble P10-1-CC, P10-1-L, and P10-1-S are shown in Fig. S9. The isotherms have complex shapes, which are not

typical for single-component surfactant solutions. The minimal experimental interfacial tension, σ_{min}, has the lowest value (below 1 mN/m) in the case of P10-1-CC solutions and the highest one (about 9 mN/m) – for P10-1-S solutions.

3.3. Phase exchange experiments and interfacial rheology

We conducted phase exchange experiments with bubbles and LMO drops (see Section 2, Figs. 5, Figs. S6 and Figs. S10) to investigate the effects of admixtures within polyglycerol esters samples on the interfacial rheology. The essential outcomes of these experiments, in terms of interfacial dilatational storage, E', and loss, E'', moduli, are collated in Tables 1, Tables S1–S3.

To characterize the properties of the P10-1-L adsorption layers, we formed a bubble in 0.05 wt% P10-1-L aqueous solution. The surface tension relaxed to 30 mN/m and the oscillatory experiments gave relatively low storage and loss moduli, 11.8 mN/m and 7.6 mN/m, respectively (run 1 in Table 1). The subsequent solution exchanges with water resulted in the increase of the surface tension to 49.6 mN/m and of the storage moduli to 40.8 mN/m (runs 2–4 in Table 1). The first hypothesis for this observation could be the formation of H-bonds between polyglycerol headgroups of adsorbed molecules. To check this, we repeated this kind of experiment using 0.05 wt% P10-1-L+1 M Urea solution and exchanged phases with 1 M Urea aqueous solution (runs 5–8 in Table 1). Key highlights from the experimental data demonstrate the significant role of urea in disrupting of the hydrogen bonding within polyglycerol esters adsorption layers. For instance, the equilibrium surface tension remains unchanged (30 mN/m) and the surface dilatational moduli have low values both before and after urea addition (as shown in runs 1 and 5 in Table 1). However, after the exchanges of the surfactant solution with 1 M Urea solution, the storage moduli, E', decrease from 40.8 mN/m to 26.9 mN/m and the loss moduli, E'', increase from 9.6 mN/m to 32.9 mN/m (runs 4 and 8 in Table 1). The lower values of the storage moduli and the higher values of the loss moduli in the presence of 1 M Urea suggest that the change of the interfacial rheology of the polyglycerol esters adsorption layers is partially attributed to the disruption of hydrogen bonds.

The second hypothesis could be the presence of traces of fatty acids in the PGE samples. To check this, first, one increases the pH of 0.05 wt% P10-1-L solutions to 8.6 and uses water at pH=8.6 for the phase exchanges (runs 9–12 in Table 1). It is seen that the storage moduli decrease before the bubble washing to 7.6 mN/m and after the phase exchanges to 14.5 mN/m compared to the respective values measured at natural pH. It is known in the literature [59], that different types of acid soups are formed in the fatty acid solutions with the rise of pH, which affect the mixed adsorption layers. Second, we added 1 mM $ZnCl_2$ to 0.05 wt% P10-1-L in order to precipitate the fatty acids (runs 13–16 in Table 1). As a result, the dilatational storage moduli drop considerably: to 4.4 mN/m before the bubble washing; to 2.6 mN/m after the phase exchanges with water. Thus, the polyglycerol esters samples contain traces of fatty acids, which affect the interfacial rheology of solutions. The high values of the loss moduli without $ZnCl_2$ and in the presence of $ZnCl_2$ show that the hydrogen bonding effect is operative mainly for the loss moduli, while the adsorbed fatty acid molecules – for the storage moduli. The analogous experiments with 0.01 wt% P10-1-CC solutions (runs 17–19 in Table 1) prove that P10-1-CC sample also contains traces of fatty acids, which adsorb irreversibly at the air/solution interfaces.

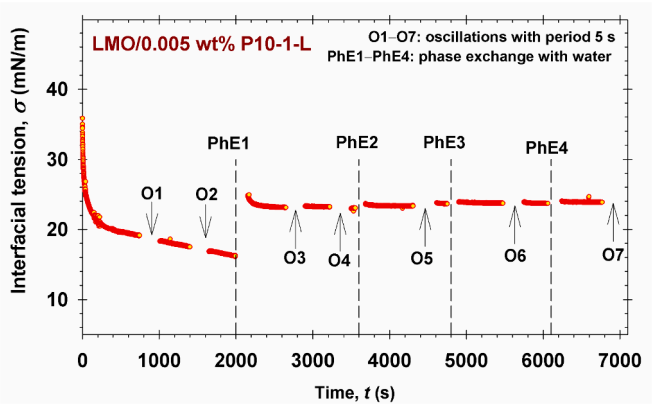

Fig. 5. Interfacial tension, σ, vs time, t, in the case of a phase exchange experiment with LMO drops. The initial concentration of P10-1-L is 0.005 wt%; four times the solutions are replaced with water (PhE1 – PhE4); seven oscillatory experiments at different times are performed (O1 – O7).

Table 1
Interfacial dilatational storage, E', and loss, E'', moduli measured at solution/air and solution/LMO interfaces by the oscillating bubble (drop) method in the case of phase exchange experiments.

Run	Systems	Stages	E', mN/m	E'', mN/m	σ, mN/m
	Solution/air				
1	0.05 wt% P10-1-L (Fig. S6)		11.8	7.6	30.0
2		1st PhE with water	39.3	19.3	44.1
3		2nd PhE with water	40.7	16.1	47.0
4		3rd PhE with water	40.8	9.6	49.6
5	0.05 wt% P10-1-L+1 M Urea (Fig. S10)		9.7	8.5	30.0
6		1st PhE with 1 M Urea	29.4	30.9	41.9
7		2nd PhE with 1 M Urea	30.2	32.9	45.4
8		3rd PhE with 1 M Urea	26.9	32.9	47.3
9	0.05 wt% P10-1-L, pH=8.6		7.6	9.8	31.7
10	1st PhE with water at pH=8.6		14.5	28.5	46.2
11	2nd PhE with water at pH=8.6		14.5	28.5	47.6
12	3rd PhE with water at pH=8.6		14.5	28.1	50.1
13	0.05 wt% P10-1-L+1 mM $ZnCl_2$, pH=8.3		4.4	10.9	30.7
14		1st PhE with water	2.1	32.4	42.1
15		2nd PhE with water	2.5	33.6	45.4
16		3rd PhE with water	2.6	34.3	47.2
17	0.01 wt% P10-1-CC		23.7	18.2	28.0
18		1st PhE with water	36.5	32	32.7
19		2nd PhE with water	42.0	27.7	35.9
	Solution/LMO				
20	0.005 wt% P10-1-L (Fig. 5)		20.2	6.6	17.4
21		1st PhE with water	25.9	1.1	23.4
22		2nd PhE with water	26.1	0.6	23.7
23		3rd PhE with water	26.6	0.5	23.5
24		4th PhE with water	25.3	0.7	24.4

A pivot finding is that even at very low concentrations (0.005 wt% P10-1-L aqueous solution), a strong elastic adsorption layer is formed at solution/LMO interface with dilatational storage and loss moduli equal to 20.2 mN/m and 6.6 mN/m, respectively (Fig. 5, runs 20–24 in Table 1). After four times of washing of the adsorption layer: the interfacial tension does not change, $\sigma = 24 \pm 0.4$ mN/m, at least for 80 min; the loss moduli have low values (below 1 mN/m); the storage moduli are approximately constant 26 mN/m. Thus, the formed adsorption layer at the water/LMO boundary has purely elastic behavior ($E' \gg E''$) which is typical for adsorbed double-tail molecules.

In summary, these experiments reveal that the studied PGEs form adsorption layers with distinct rheological properties influenced by the presence of double-tail molecules and admixtures of fatty acids. The observed behavior reflects the complex interplay between the surfactant concentration, admixture composition, and the resultant interfacial properties.

4. Thin liquid films

To study the interactions between adsorbed layers, we performed thin foam film experiments with polyglycerol esters solutions using the SE capillary cell (Section 2). Fig. S12 summarizes the dependencies of the film thickness, h, on time t for P10-1-CC and P10-1-L aqueous solutions. The first equilibrium thicknesses correspond to the first

conditionally stable gray films, which could be formed in the SE cell. One sees that the films stabilized with 0.2 wt% P10-1-CC and P10-1-L are thick with identical first equilibrium thicknesses of 95 nm. In the case of 1.0 wt% P10-1-L, the respective equilibrium thickness drops to 58 nm. These thicknesses typically are explained with the electrostatic repulsion between charged adsorption layers. Because of fluctuations, the electrostatic barrier can be overcome, subsequently the foam film drainages, and darker spots appear in the film with a thickness corresponding to the second equilibrium thickness. The direct prove of the electrostatic nature of the disjoining pressure is the behavior of the analogous thin foam films when 100 mM NaCl is added to the respective surfactant solutions. The electrostatic barrier disappears in the presence of salt and as a result: i) the drainage rate considerably increases; ii) the first equilibrium film thickness disappears; iii) the second equilibrium film thicknesses with and without added salt practically coincide. When one has turbid solutions, it is possible to observe aggregate caught in the film which are visualized like dots or lumps in the film (see Fig. S14). In the case of P10-1-CC and P10-1-L, there are no visible aggregates caught in the film. All aggregates are expelled from the film region upon its thinning.

The phase exchange experiments show that the polyglycerol esters samples contain traces of fatty acids with $pK_a = 4.7$ [59]. At the natural pH (about 6) of the surfactant solutions, the fatty acids are ionized. If the pH of P10-1-L solutions is adjusted to 3.7, the fatty acids molecules become protonated, i.e. neutral, the electrostatic repulsion disappears and the equilibrium film thicknesses decrease to approximately 10 nm (see Fig. 6a and Fig. S13). At high ionic strengths and at pH=3.7, the foam films drainage to the final equilibrium film thickness corresponding to the surfactant bilayer formation.

If the capillary pressure, p_c, in the SE capillary cell ($p_c = 50$ mN/m) becomes equal to the disjoining pressure, Π, then the foam film reaches its equilibrium thickness. At $h > 15$ nm, the main contributions in Π come from both the van der Waals attraction component, Π_{vdW}, and from the electrostatic repulsion component, Π_{el}. That is

$$p_c = \Pi_{vdW} + \Pi_{el} \tag{6}$$

Here:

$$\Pi_{vdW} = -\frac{A_H}{6\pi h^3}\ , \quad \Pi_{el} = 64 k_B T I \tanh^2\left(\frac{\Phi_s}{4}\right)\exp(-\kappa h) \tag{7}$$

$A_H = 4 \times 10^{-20}$ J is the Hamaker constant; I is the ionic strength; κ is the inverse Debye screening length; Φ_s is the dimensionless surface electrostatic potential. The expression for Π_{el} in Eq. (7) corresponds to the approximation valid for 1:1 electrolyte at $\kappa h \gg 1$ [60]. The electrolytic conductivity experiments (see Fig. S2) showed that the slopes of the conductivity vs concentration are equal to 5.17 ± 0.01 S cm^{2}mol^{-1} for P10-1-CC and 4.91 ± 0.01 S cm^{2}mol^{-1} for P10-1-L aqueous solutions. If one assumes that these slopes correspond to the ionized fatty acids in the samples, then one obtains that the mole fraction of fatty acids in P10-1-CC is equal to 6.7 % and that in P10-1-L is 6.5 %. Thus, the only unknown parameter in Eqs. (6) and (7) is the value of the electrostatic potential at the film surfaces. The solid lines in Fig. 6 show the best theoretical fits with surface potentials of -60.2 ± 0.4 mV for foam films stabilized with P10-1-CC solutions at a natural pH and -51.3 ± 0.2 mV in the case of P10-1-L solutions. This is an independent proof that the traces of fatty acids affect not only the interfacial rheology (Section 3.3) but also the stability and drainage of foam films.

Fig. 7 shows photographs of the thinning process of a foam film formed in the SE capillary cell from 20 wt% P10-1-L solution at a natural pH. The stepwise decrease of the film thickness (stratification) occurs through formation and expansion of spots of smaller thickness in the film [54]. Each metastable state of a given uniform thickness, denoted as h_1, h_2, and h_3, corresponds to a given number of micellar layers within the film. In reflected light, the films appear grey; the thinner films look darker. In our case, the final stable state, h_1, corresponds to one layer of micelles. The thicknesses of the respective metastable states, as determined, are: $h_1 = 30.6$ nm; $h_2 = 45.7$ nm; $h_3 = 61.1$ nm. Usually, the second equilibrium thicknesses (10 ± 0.2 nm in Fig. 6) are very close to the thicknesses of surfactant bilayers. The mean heights of the stratification steps (15.2 ± 0.1 nm) represent the hydrodynamic diameter of the surfactant micelles because the stepwise thinning corresponds to the expelling of one layer of micelles from the film region. Thus, the P10-1-L micelles are ellipsoidal and slightly elongated.

The foam films stabilized with 1 wt% P10-1-S solution at a natural pH are stable in a closed SE capillary cell (at low applied p_c), see Fig. S14. They contain aggregates which are due to the limited solubility of the contained components. Upon water evaporation in an open cell at high pressure differences, these films are unstable and break – the aggregates exhibit an antifoaming action. In contrast, the films stabilized with 1 wt% P10-1-O aqueous solutions at a natural pH are thick and stable both in closed and open cells (Fig. S15), which correlates with the foam stability in a sparging regime, see Section 5.2. There are no visible aggregates caught between the film surfaces. In foaming under a stirring regime, no foam is generated from the P10-1-O solutions. This could be explained with solidified and fragile adsorption layers, which break (and do not regenerate) upon stirring and delayed surface adsorption (see Section 5).

5. Dynamic surface tension and foam properties

5.1. Dynamic surface tensions of polyglycerol esters solutions

The measured by MBPM dependencies of the dynamic surface tensions, σ, on the experimental bubbling time, t_{age}, are summarized in Fig. 8a, Fig. 8b, and Fig. S16 for different concentrations of PGE

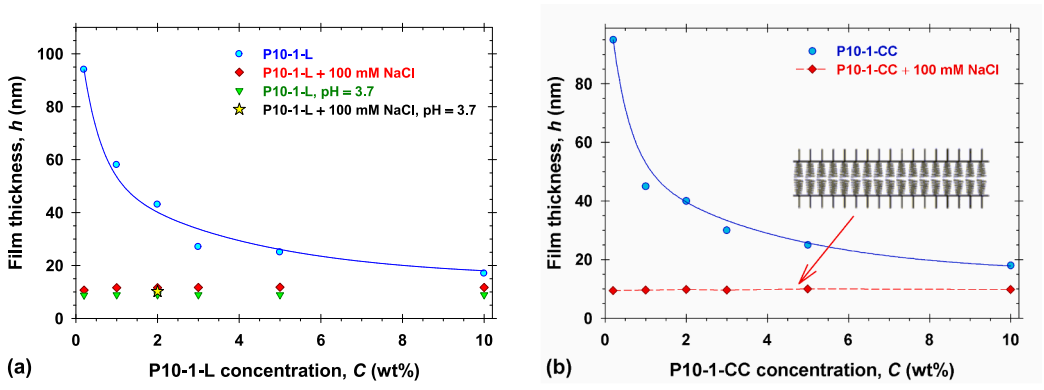

Fig. 6. Equilibrium foam film thickness, h, vs surfactant concentration, C: a) P10-1-L; b) P10-1-CC. The solid line corresponds to the theoretical calculations using the electrostatic and van der Waals components of the disjoining pressure.

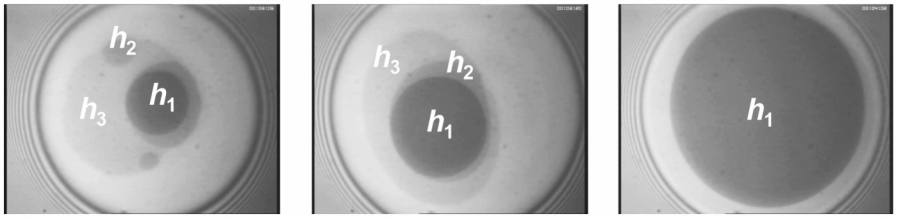

Fig. 7. Consequent stages of thinning of stratifying foam film stabilized with 20 wt% P10-1-L solution at a natural pH. The thicknesses of the metastable films are h_1, h_2, and h_3.

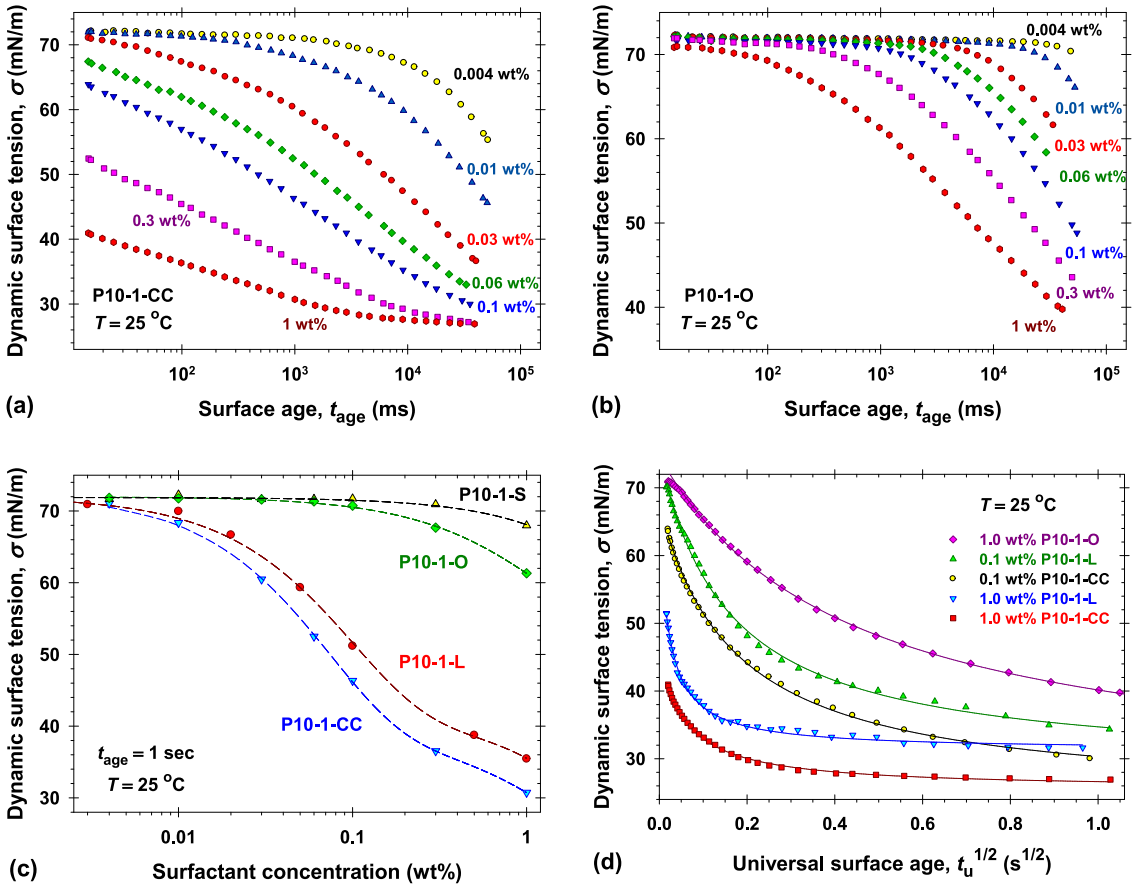

Fig. 8. Dynamic surface tensions of polyglycerol esters aqueous solutions vs the surface age, t_{age}, measured for different surfactant concentrations: a) P10-1-CC; b) P10-1-O. c) Comparison between the dynamic surface tensions measured at $t_{age} = 1$ *sec* and different concentrations of polyglycerol esters. d) Determination of the characteristic adsorption times, t_a, for 0.1 wt% and 1.0 wt% P10-1-CC and P10-1-L and for 1.0 wt% P10-1-O solutions.

solutions. As one can expect, the relaxation of $\sigma(t_{age})$ and the dynamic adsorption processes are faster for the higher surfactant concentrations. For a fixed surfactant concentration, the characteristic adsorption time increases in the order P10-1-CC<P10-1-L<P10-1-O<P10-1-S, which correlates with the relaxation of surface tension measured under static conditions, see Fig. 2. For example, if one plots the dynamic surface tension measured at $t_{age} = 1$ *sec* vs surfactant concentration (Fig. 8c), then one sees that this trend is more pronounced for surfactant concentrations higher than 0.03 wt%, while for lower concentrations, the moment values of the dynamic adsorptions are low and one expects a low foaming ability of polyglycerol esters solutions.

It has been shown in the literature, that the bubble surfaces are continuously expanded in the case of MBPM and the nominal surface age at the moment of maximum pressure, t_{age}, is equivalent by adsorption to initially clean immobile surface of age, t_u, known as a universal surface age [52]. Note, that t_{age} depends on the used MBPM apparatus, while t_u is an independent characteristic of the adsorption processes (in our case $t_u = t_{age}/37$). Moreover, based on the long-time asymptotic behavior of the surface tension, the authors [52] obtained the following relationship:

$$\sigma(t_u) \approx \frac{a + \sigma_{eq} t_u^{1/2}}{t_a^{1/2} + t_u^{1/2}} \tag{8}$$

Here: σ_{eq} is the equilibrium surface tension; a is a constant, which depends on the experimental conditions; t_a is the characteristic adsorption time, which is a physicochemical parameter of the respective solution at a given concentration and temperature. Fig. 8d shows the experimental data and the best theoretical fits according to Eq. (8). In all illustrated cases, the regression coefficients are larger than 0.9998 and the relative errors of the most probable values of t_a are lower than 0.01. Note that for low surfactant concentrations and for all studied concentrations of P10-1-S, the longest experimental time realized by BP 100, t_{age}, is not enough

to apply the long-time asymptotic formula, Eq. (8).

Table 2 summarizes the obtained results for the initial foam heights, H_f, and the characteristic adsorption times, t_a, for polyglycerol esters solutions at concentrations 0.1 wt% and 1.0 wt%. It is well illustrated that H_f increases with the decrease of t_a in both stirring and sparging regimes of a foam formation. The only exception is the foaming ability of P10-1-O aqueous solutions. In the sparging regime, P10-1-O aqueous solutions produce foams, which correlates with the thin liquid films stability (see Section 4). In the stirring regime, there is no foam formation from P10-1-O solutions most probably due to the solidified and fragile adsorption layers.

5.2. Stability of foams produced from polyglycerol esters solutions

Stirring regime. One of the quantitative characteristics of the foam stability is the so-called bubble count diagram. It represents the time dependence of the numbers of bubbles, having projection areas in given ranges, per unit area. In the case of stirring regime, Fig. 9a and 9b show these experimental dependencies for foams stabilized with 0.1 wt% and 1.0 wt% P10-1-L solutions and Figs. S17a and S17b for P10-1-CC solutions, respectively. Pictures of these foams taken close to the solution/foam boundary after 30 min from the foam formation are summarized in Table S4. It is well illustrated, that the area occupied by all bubbles of area smaller than 0.1 mm^2 begins to continuously diminish soon after the foam formation. Thus, the foam disproportionation because of the Ostwald ripening takes place [61]. At 1 wt% P10-1-L, the slope of the curve with bubble areas smaller than 0.1 mm^2 (Fig, 9b) is lower than that for 0.1 wt% (Fig. 9a) and the Ostwald ripening is slower. The fractions of bigger bubbles (in the ranges $0.1 - 0.2\ mm^2$; $0.2 - 0.3\ mm^2$; $> 0.3\ mm^2$) continuously increase and level off due to the bubble coalescence. Note that the fraction of bubbles with areas greater than 0.3 mm^2 does not appear even after 30 min for the foam stabilized with 1.0 wt% P10-1-L (Fig. 9b) – this foam is more stable than that produced from 0.1 wt% P10-1-L. The bubble count diagrams for the foams stabilized with both P10-1-CC concentrations (Fig. S17) are quite similar to that shown in Fig. 9a. Thus, these foams are unstable and the Ostwald ripening and bubble coalescence are observed for both P10-1-CC solutions. In contrast, the foams stabilized with 0.1 wt% and 1.0 wt% P10-1-S are stable – the mean bubble size does not change up to 30 min. Note that the foaminess of polyglycerol esters solutions is different and depends on the surfactant concentration, the length of the hydrocarbon tail, and the characteristic adsorption time (see Table 2).

The dependencies of the average bubble radius, R_{ave} (calculated from the bubble count diagrams), on the polyglycerol esters concentrations and time t are summarized in Fig. 9c and 9d. The initial values of R_{ave} are about 0.1 mm for the foams stabilized both with P10-1-CC and P10-1-L at 0.1 wt% and 1.0 wt%, while in the case of P10-1-S, it is larger (0.14 mm) and increases insignificantly for the period of observation. The foam coarsening for the lower surfactant concentration (0.1 wt%) of P10-1-CC and P10-1-L (see Fig. 9c) is practically identical: i) R_{ave} does not change for the first 5 min; ii) the linear increase of R_{ave} with time is measured for $t > 5$ min. For 1 wt% (Fig. 9d), the initial lag time extends to 7 min for P10-1-CC and to 9 min for P10-1-L. The respective slope of R_{ave} for the longer times with P10-1-L is smaller and the foam is more stable than that stabilized with P10-1-CC.

Table 2
The initial foam heights, H_f, and the characteristic adsorption times, t_a, of polyglycerol esters solutions at concentrations 0.1 wt% and 1.0 wt%.

	H_f (stirring)		H_f (sparging)		t_a (MBPM)	
	0.1 wt%	1.0 wt%	0.1 wt%	1.0 wt%	0.1 wt %	1.0 wt%
P10-1-CC	22 (mm)	56 (mm)	67 (mm)	170 (mm)	25 (ms)	0.53 (ms)
P10-1-L	17 (mm)	44 (mm)	54 (mm)	140 (mm)	30 (ms)	3.1 (ms)
P10-1-O	–	2 (mm)	51 (mm)	120 (mm)	–	187 (ms)
P10-1-S	5 (mm)	36 (mm)	53 (mm)	140 (mm)	–	–

To show the possibility to combine the good foaminess of P10-1-CC and the foam stability properties of P10-1-S, we studied the effect of mixed P10-1-CC and P10-1-S surfactant solutions with total concentration 1 wt% on the foamability and foam stability using a stirring regime. Fig. 10a and 10b show that the foam height, H_f, and the mean bubble radii, R_{32}, of foam produced from 1 wt% P10-1-S aqueous solution do not change at least for 30 min, but the foam height is relatively low. The addition of even small amount of P10-1-CC, e.g. 10:1 (w/w) P10-1-S:P10-1-CC, increases H_f more than 25 % (Fig. 10a), decreases the initial bubble radius from 70 μm to 50 μm (Fig. 10b), but the Ostwald ripening effect arises – the mean bubble radius rises to 80 μm for 30 min. It is important to note that the increase of the P10-1-CC weight fraction up to 7:4 (w/w) practically does not change the initial foam volume but it affects the foam coarsening – R_{32} increases faster for higher P10-1-CC weight fractions. Pictures of respective foams taken after 30 min are summarized in Table S5. Thus, the fine balance between P10-1-CC and P10-1-S can be used to produce foams with a preferred properties for different practical applications.

It is also possible to combine P10-1-O (which does not produce foams in a stirring regime) and P10-1-CC to obtain relatively stable foams, see Table S6 and Fig. S18. In the case of 1 wt% total surfactant concentration, the smallest value of the mean bubble radius, $R_{32} = 180$ μm, is observed for 7:4 (w/w) P10-1-O:P10-1-CC. The measured foam volumes after 30 min monotonically increase with the rise of the P10-1-CC weight fraction. In contrast to P10-1-S, the usage of P10-1-O and P10-1-CC mixtures has no definite advantages with respect to the foam production in a stirring regime.

Sparging regime. For our study of the foamability in sparging regime, we used low flow rate of 0.4 dm^3/min (Section 2) and times of bubbling until reaching 220 mm foam height in all cases reported below. The mixed surfactant solutions properties are illustrated in Figs. S19 and S20: i) the solubility of P10-1-S and P10-1-O in P10-1-CC and P10-1-L decreases with the rise of weight fractions of P10-1-S and P10-1-O; ii) there is no visible difference between P10-1-CC and P10-1-L in the respective mixed surfactant solutions; iii) the turbidity of P10-1-O containing solutions is lower than that of P10-1-S mixed solutions at a fixed weight fraction of P10-1-O or P10-1-S.

The stability of foams produced from P10-1-S containing mixed surfactant solutions is summarized in Figs. S21-S23, Fig. 11a, and Fig. 11b. For a fixed total surfactant concentration, C_T=1 wt%: i) the initial bubble radii, R_{32}, for P10-1-S alone are the largest (280 μm) and only slightly increase in time up to 15 min storage time; ii) for all weight fractions of P10-1-CC or P10-1-L larger than 0.1, the initial bubble radii, R_{32}, are considerably lower and approximately equal (≈ 80 μm); iii) the slopes, R_{32} vs t, increase with the rise of P10-1-CC or P10-1-L weight fractions. Thus, from the viewpoint of the slowest change of the bubble radii in the foams, the optimal choice is the foams produced in a sparging regime from 9:1 (w/w) P10-1-S with P10-1-CC or P10-1-L mixed surfactant solutions.

The optimization of this composition, 9:1 (w/w) P10-1-S with P10-1-CC or P10-1-L, with respect to the total surfactant concentration is summarized in Figs. S23, Fig. 11a, and Fig. 11b. In the case of 9:1 (w/w) P10-1-S:P10-1-CC: i) the foams are unstable for low concentrations, C_T<0.08 wt%; ii) they are also unstable for high concentrations, $C_T \geq 2.5$ wt% – the precipitates have an antifoaming effect; iii) for 0.8 wt% ≤ C_T<2.5 wt%, dR_{32}/dt has a minimum at a given total surfactant concentration. The main difference in the case of 9:1 (w/w) P10-1-S:P10-1-L is that the foams are stable up to the highest studied concentration, C_T=5 wt%. The minimal initial values of the mean bubble radii, $R_{32,in}$, and the total surfactant concentrations at which $R_{32,in}$ are measured, $C_{T,in}$, are summarized in Table 3. It well illustrates that $R_{32,in}$ is approximately constant, but $C_{T,in}$ is considerably larger for P10-1-L containing

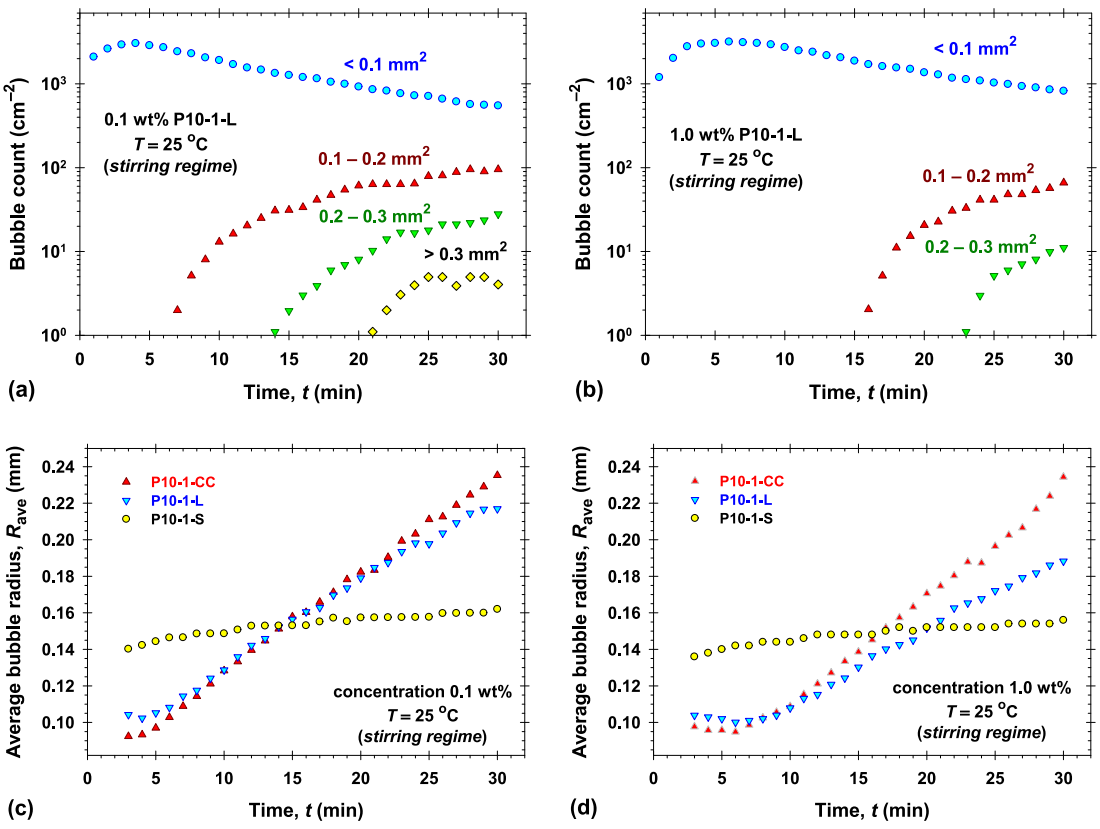

Fig. 9. Change of the numbers of bubbles, having projection areas in given ranges, per unit area vs time in a stirring regime: a) 0.1 wt% P10-1-L aqueous solution; b) 1.0 wt% P10-1-L aqueous solution. Dependence of the average bubble radius, R_{ave}, on time for foams produced in a stirring regime and stabilized with different polyglycerol esters: c) 0.1 wt% surfactant solution; d) 1.0 wt% surfactant solution.

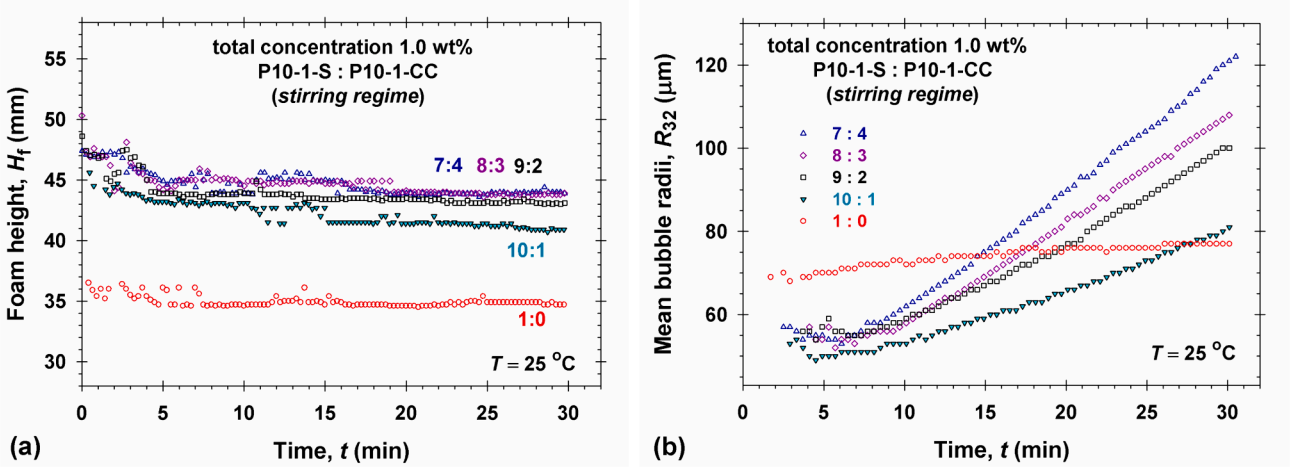

Fig. 10. Foam height (a) and mean bubble radii (b) vs time of foams stabilized with 1.0 wt% total concentration of mixed P10-1-S and P10-1-CC surfactant solutions. All foams are produced in a stirring regime.

solutions compared to P10-1-CC. The respective parameters measured after 15 min, $R_{32,fin}$ and $C_{T,fin}$, listed in Table 3 show that the foams stabilized with P10-1-S+P10-1-L solutions in a sparging regime are again more stable as it was in a stirring regime.

The foam properties of P10-1-O and P10-1-CC or P10-1-L mixed surfactant solutions in a sparging regime are analogous to those for P10-1-S. The main difference is that these mixed solutions produced foams even at larger concentrations, C_T=5 wt%, because of their lower turbidity compared to P10-1-S. Nevertheless, the mean bubble radii, $R_{32,in}$ and $R_{32,fin}$, are more than two times larger compared to those in the case of P10-1-S, see Fig. 11 and Table 3. This fact correlates with the respective observations in a stirring regime.

6. Conclusions

In spite of the wide application of the polyglycerol esters of fatty acids (PGE) in the diverse industries, cosmetics, and medicine [1,3,12–23], their colloid and interface properties are not well revealed [9,32,38,46–48]. The complexity of PGE and their wide range of colloid and interface properties arise from the polymerization process of

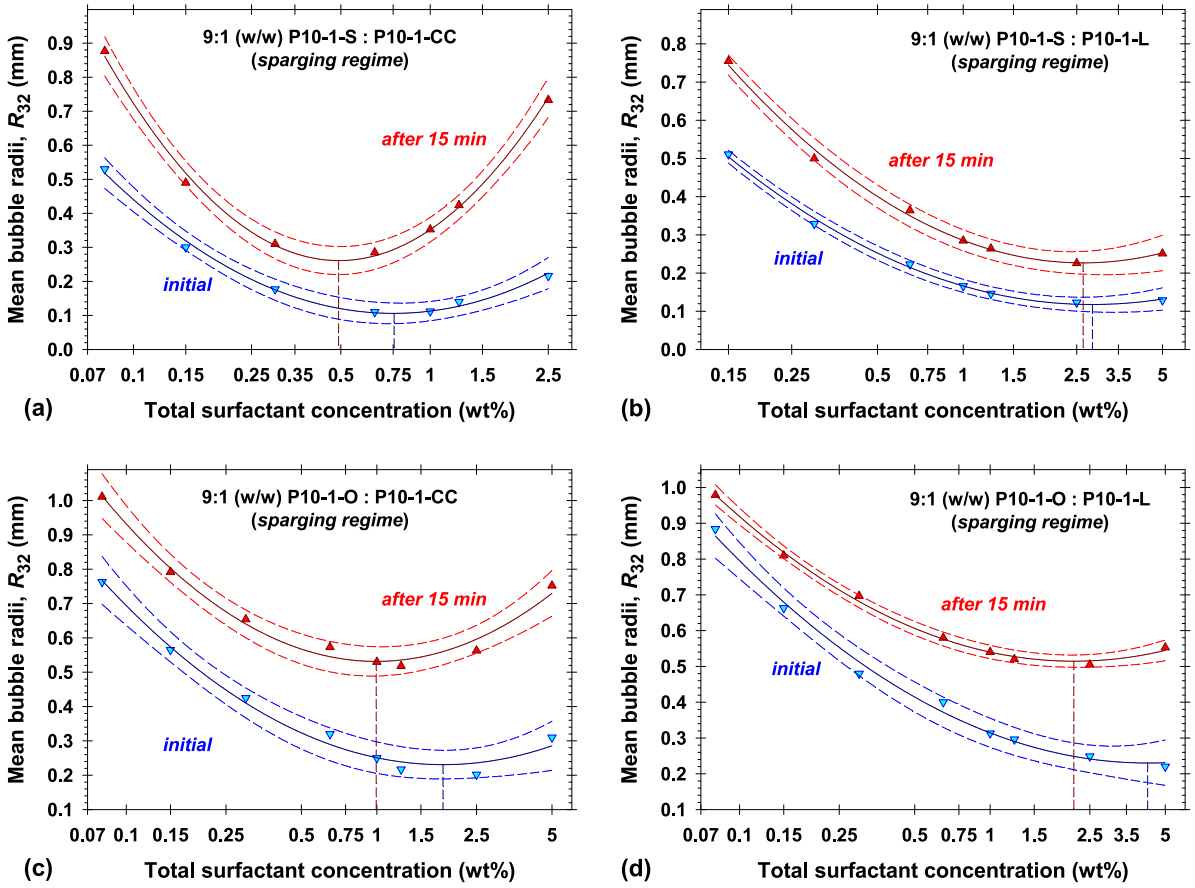

Fig. 11. Dependence of the initial mean bubble radii, R_{32}, and those measured after 15 min on the total surfactant concentration for foams produced in a sparging regime from mixed solutions of: a) 9:1 (w/w) P10-1-S:P10-1-CC; b) 9:1 (w/w) P10-1-S:P10-1-L; c) 9:1 (w/w) P10-1-O:P10-1-CC; d) 9:1 (w/w) P10-1-O:P10-1-L. The dashed lines correspond to the 95% confidential band around the experimental data. The vertical dashed lines show the positions of the minimal radii.

Table 3
The positions and values of the minimal mean bubble radii, R_{32}, for foams stabilized with 9:1 (w/w) P10-1-S or P10-1-O and P10-1-CC or P10-1-L surfactant solutions in a sparging regime, see Fig. 11.

	$C_{T,in}$ (wt%)	$R_{32,in}$ (mm)	$C_{T,fin}$ (wt%)	$R_{32,fin}$ (mm)
P10-1-S+P10-1-CC	0.756	0.106	0.491	0.261
P10-1-S+P10-1-L	2.84	0.118	2.63	0.227
P10-1-O+P10-1-CC	1.84	0.231	0.994	0.532
P10-1-O+P10-1-L	4.25	0.230	2.16	0.515

polyglycerol, which results in the production of various oligomers [1–7]. For the physicochemical characterization of PGEs solutions, one can combine complementary experimental techniques and adequate theoretical interpretation of the obtained results.

Polyglycerol mono-laurate (P10-1-L), mono-stearate (P10-1-S), mono-oleate (P10-1-O), and an equimolar mixture of mono-caprylate and mono-caprate (P10-1-CC) esters samples are well-soluble in water. They contain minuscule concentration of indifferent electrolyte, low molar fractions of fatty acid and dual-hydrocarbon-tailed polyglycerol esters molecules (Secs. 2,3,4). The combination of DLS, SLS, turbidity, and interfacial tension measurements characterize their self-aggregation and adsorption properties. P10-1-CC aqueous solutions are turbid for concentration between 0.3 wt% and 2.0 wt% because of the effect of 0.31 mol% of double-tail esters on the formation of vesicular structures. With the increase of the single-tail esters concentration, the double-tail esters are solubilized in the micelles and the solutions become transparent (*Sec*. 3). The kink point in the P10-1-CC surface tension isotherm at 0.001 wt% is lower than that measured in the literature [32] and corresponds to the critical aggregate bulk concentration (CAC). The relatively high saturation adsorption (4.76 μmol/m^2) and interfacial interaction parameter (5.5), as well as the effect of added 1 M Urea or 1 mM $ZnCl_2$, clarify the importance of the H-bonds between polyglycerol head groups of adsorbed molecules on the interfacial dilatational loss moduli and that of the fatty acid admixture on the storage moduli. In contrast, the considerably lower number of double-tail esters in P10-1-L, P10-1-S, and P10-1-O prevents the vesicle formation and the turbidity of aqueous solutions monotonically increase with concentration. As a result, the saturation adsorption of P10-1-L is 4.42 μmol/m^2, the interaction parameter is four times lower than that of P10-1-CC, and the CAC if five times lower compared to the purified polyglyceryl mono-laurate [47]. The saturation adsorption of longer chain length PGE (2.81 μmol/m^2) is closed to the literature data. The solubility of P10-1-O in both water and oily phases leads to its spontaneous emulsification ability, low interfacial tension (below 0.7 mN/m), and good emulsification properties.

The measurements of the dynamics, stability and stratification of thin liquid film stabilized with PGE complement the information on the interaction of the adsorbed layers (*Sec*. 4). The dependence of the first equilibrium thickness of films stabilized with P10-1-CC and P10-1-L on the surfactant concentration demonstrates the effect of the electrostatic interactions because of the fatty acid admixtures (Fig. 6). The calculated surface electrostatic potentials are varied from − 50 mV to − 60 mV. The presence of 100 mM NaCl or the decrease of the pH to 3.7 lead to stable films with equilibrium thickness of 10 nm. The size of the stratification steps of 15 nm at larger PGE concentrations (Fig. 7) suggests the presence of elongated ellipsoidal micelles in P10-1-CC and P10-1-L aqueous solutions. The P10-1-S stabilized films contain aggregates due to the

limited solubility of the components, which break the foam films at a high applied capillary pressure. In contrast, P10-1-O solutions form relatively thick and stable films without aggregates caught between film surfaces.

The correlation between the characteristic adsorption time obtained in the dynamic surface tension experiments and the foamability of PGE solutions in stirring and sparging regimes (Table 2) explains the good foaming properties of the short chain length PGEs. The bubble count diagrams (Fig. 9) quantitatively explain the effect of Ostwald ripening and bubble coalescence on the increase of initial bubble size (100 μm) with time in a time scale of 30 min. P10-1-S foams are characterized with larger bubble sizes (140 μm), lower foam volumes, and the absence of the Ostwald ripening and bubble coalescence. The combination of the liquid and interface properties of C10-1-CC (C10-1-L) with those of C10-1-S leads to optimization of foam from mixed surfactant solutions upon foamability and foam stability with respect to concentration and weight fraction of components (Figs. 10 and 11).

The proposed experimental and theoretical approach is applicable for the characterization of liquid and interface properties of commercially available water-soluble surfactants with complex structures. The reported physicochemical characterization of studied water-soluble polyglycerol esters could be of interest to increase the range of their applicability in practice.

CRediT authorship contribution statement

Rumyana D. Stanimirova: Writing – original draft, Investigation, Data curation. **Krassimir D. Danov:** Supervision, Software, Formal analysis. **Mihail T. Georgiev:** Investigation, Data curation. **Jordan T. Petkov:** Supervision, Methodology, Conceptualization.

Declaration of competing interest

The authors declare that they have no known competing financial interests or personal relationships that could have appeared to influence the work reported in this paper.

Data availability

Data will be made available on request.

Acknowledgements

The authors are grateful to the project № КП-06-ПН 49/5 with the Bulgarian Science Fund (FNI-MON) for the financial support.

Appendix A. Supplementary data

Supplementary data to this article can be found online at https://doi.org/10.1016/j.jcis.2024.07.219.

References

[1] W. Hemker, Associative structures of polyglycerol esters in food emulsions, J. Am. Oil Chem. Soc. 58 (1981) 114–119, https://doi.org/10.1007/BF02672194.
[2] R. Mclntyre, Polyglycerol esters, J. Am. Oil Chem. Soc. 56 (1979) 835A–A840, https://doi.org/10.1007/BF02667458.
[3] V. Norn, Polyglycerol esters, in: V. Norn (Ed.), Emulsifiers in Food Technology, Wiley-Blackwell, Denmark, 2015, Ch. 8, pp. 181–208, Doi: 10.1002/9781118921265.ch8.
[4] H.S. Usha, S. Maitra, Synthesis characterization and application of polyglycerol esters of fatty acids: biodegradable surfactants, J. Dispers. Sci. Technol. 37 (2016) 41–47, https://doi.org/10.1080/01932691.2015.1025137.
[5] Z. Fan, Y. Zhao, F. Preda, J.-M. Clacens, H. Shi, L. Wang, X. Feng, F. De Campo, Preparation of bio-based surfactants from glycerol and dodecanol by direct etherification, Green Chem. 17 (2015) 882–892, https://doi.org/10.1039/C4GC00818A.
[6] O. Valerio, M. Misra, A.K. Mohanty, Poly(glycerol-co-diacids) polyesters: from glycerol biorefinery to sustainable engineering applications, A review, ACS Sustainable Chem. Eng. 6 (2018) 5681–5693, https://doi.org/10.1021/acssuschemeng.7b04837.
[7] K.S. Shikhaliev, N.V. Stolpovskaya, M.Y. Krysin, A.V. Zorina, D.V. Lyapun, F. I. Zubkov, K.Y. Yankina, Production and emulsifying effect of polyglycerol and fatty acid esters with varying degrees of esterification, J. Am. Oil Chem. Soc. 93 (2016) 1429–1440, https://doi.org/10.1007/s11746-016-2894-6.
[8] B. Peng, C.-Y. Xiong, Y. Huang, J.-N. Hu, X.-M. Zhu, Z.-Y. Deng, Enzymatic synthesis of polyglycerol fatty acid esters and their application as emulsion stabilizers, J. Agric. Food Chem. 66 (2018) 8104–8113, https://doi.org/10.1021/acs.jafc.8b00222.
[9] S. Holmiere, R. Valentin, P. Maréchal, Z. Mouloungui, Esters of oligo-(glycerol carbonate-glycerol): new biobased oligomeric surfactants, J. Colloid Interface Sci. 487 (2017) 418–425, https://doi.org/10.1016/j.jcis.2016.10.072.
[10] M. Friedman, N. Garti, Preparation and surface properties of new sulfosuccinic derivatives of fatty polyglycerol esters, J. Dispers. Sci. Technol. 10 (1989) 285–306, https://doi.org/10.1080/01932698908943177.
[11] M.M. Flume, W.F. Bergfeld, D.V. Belsito, R.A. Hill, C.D. Klaasen, D.C. Liebrer, J. G. Marks, R.C. Shank, T.J. Slaga, P.W. Snyder, L.J. Gill, B. Heldreth, Safety assessment of polyglyceryl fatty acid esters as used in cosmetics, Int. J. Toxicol. 42 (2023) 5S–101S, https://doi.org/10.1177/10915818231174440.
[12] K. Matsumoto, K. Matsumoto, Development of W/O emulsion to form harmless ice slurry to human being, Int. J. Refrig. 32 (2009) 411–420, https://doi.org/10.1016/j.ijrefrig.2008.09.005.
[13] K. Matsumoto, D. Shirai, Y. Furudate, D. Tsubaki, H. Kubota, K. Sekine, K. Minamiya, Active control of supercooling degree using surfactant (In system with solid-liquid interface), Int. J. Refrig. 58 (2015) 199–206, https://doi.org/10.1016/j.ijrefrig.2015.05.010.
[14] K. Matsumoto, Y. Igarashi, D. Shirai, K. Hayashi, Investigation of the influence of surfactant on the degree of supercooling (coexisting system of solid-liquid and gas-liquid interfaces), Int. J. Refrig. 36 (2013) 1302–1309, https://doi.org/10.1016/j.ijrefrig.2013.02.007.
[15] F.C. Wang, A.G. Marangoni, Advances in the application of food emulsifier α-gel phases: saturated monoglycerides, polyglycerol fatty acid esters, and their derivatives, J. Colloid Interface Sci. 483 (2016) 394–403, https://doi.org/10.1016/j.jcis.2016.08.012.
[16] A. Ogawa, H. Cho, Role of food emulsifiers in milk coffee beverages, J. Colloid Interface Sci. 449 (2015) 198–204, https://doi.org/10.1016/j.jcis.2015.01.063.
[17] F.F. Sahle, H. Metz, J. Wohlrab, R.H.H. Neubert, Polyglycerol fatty acid ester surfactant-based microemulsions for targeted delivery of ceramide AP into the stratum corneum: Formulation, characterization, *in vitro* release and penetration investigation, Eur. J. Pharm. Biopharm. 82 (2012) 139–150, https://doi.org/10.1016/j.ejpb.2012.05.017.
[18] D. Köpke, S.M. Pyo, Symurban nanocrystals for advanced anti-pollution skincare, Cosmetics 7 (2020) 17, https://doi.org/10.3390/cosmetics7010017.
[19] S. Hönzke, C. Gerecke, A. Elpelt, N. Zhang, M. Unbehauen, V. Kral, E. Fleige, F. Paulus, R. Haag, M. Schäfer-Korting, B. Kleuser, S. Hedtrich, Tailored dendritic core-multishell nanocarriers for efficient dermal drug delivery: a systematic top-down approach from synthesis to preclinical testing, J. Control. Release 242 (2016) 50–63, https://doi.org/10.1016/j.jconrel.2016.06.030.
[20] A. Huynh, A.G. Garcia, L.K. Young, M. Szoboszlai, M.W. Liberatore, G. Baki, Measurements meet perceptions: rheology-texture-sensory relations when using green, bio-derived emollients in cosmetic emulsions, Int. J. Cosmet. Sci. 43 (2021) 11–19, https://doi.org/10.1111/ics.12661.
[21] W.-K. Fong, R. Negrini, J.J. Vallooran, R. Mezzenga, B.J. Boyd, Responsive self-assembled nanostructured lipid systems for drug delivery and diagnostics, J. Colloid Interface Sci. 484 (2016) 320–339, https://doi.org/10.1016/j.jcis.2016.08.077.
[22] S. Park, S. Mun, Y.T. Kim, Influences of added surfactants on the water solubility and antibacterial activity of rosemary extract, Food Sci. Biotechnol. 29 (2020) 1373–1380, https://doi.org/10.1007/s10068-020-00792-w.
[23] Y.J. Hao, S.M. Huey, Y.C. Beng, S. Kanagaratnam, L.C. Abdullah, T.C.S. Yaw, The effects of polyglycerol esters on palm olein fractionation, J. Oil Palm Res. 31 (2019) 294–303, https://doi.org/10.21894/jopr.2019.0015.
[24] R. Katoh, Y. Asano, A. Furuya, K. Sotoyama, M. Tomita, Preparation of food emulsions using a membrane emulsification system, J. Memb. Sci. 113 (1996) 131–135, https://doi.org/10.1016/0376-7388(95)00227-8.
[25] G. De Luka, E. Drioli, Force balance conditions for droplet formation in cross-flow membrane emulsifications, J. Colloid Interface Sci. 294 (2006) 436–448, https://doi.org/10.1016/j.jcis.2005.07.055.
[26] T. Schmidts, D. Dobler, C. Nissing, F. Runkel, Influence of hydrophilic surfactants on the properties of multiple W/O/W emulsions, J. Colloid Interface Sci. 338 (2009) 184–192, https://doi.org/10.1016/j.jcis.2009.06.033.
[27] M. Matos, G. Gutiérrez, J. Coca, C. Pazos, Preparation of water-in-oil-in-water ($W_1/O/W_2$) double emulsions containing *trans*-resveratrol, Colloids Surf. A 442 (2014) 69–79, https://doi.org/10.1016/j.colsurfa.2013.05.065.
[28] M. Shima, Y. Kobayashi, Y. Kimura, S. Adachi, R. Matsuno, Effect of the hydrophilic surfactants on the preparation and encapsulation efficiency in course and fine W/O/W type emulsions, Colloids Surf. A 238 (2004) 83–90, https://doi.org/10.1016/j.colsurfa.2004.02.018.
[29] S. Herzi, W. Essafi, S. Bellagha, F. Leal-Calderon, Influence of the inner droplet fraction on the release rate profiles from multiple W/O/W emulsions, Colloids Surf. A 441 (2014) 489–495, https://doi.org/10.1016/j.colsurfa.2013.09.036.
[30] N. Prichapan, D.J. McClements, U. Klinkesorn, Iron encapsulation in water-in-oil emulsions: effect of ferrous sulfate concentration and fat crystal formation on oxidative stability, J. Food Sci. 83 (2018) 309–317, https://doi.org/10.1111/1750-3841.14034.

[31] S. Wald, J. Simon, J.P. Dietz, F.R. Wurm, K. Landfester, Polyglycerol surfmers and surfactants for direct and inverse mini emulsion, Macromol. Biosci. 17 (2017) 1700070, https://doi.org/10.1002/mabi.201700070.
[32] L. Pavoni, D.R. Perinelli, A. Ciacciarelli, L. Quassinti, M. Bramucci, A. Miano, L. Casettari, M. Cespia, G. Bonacucina, G.F. Palmieri, Properties and stability of nanoemulsions: how relevant is the type of surfactant? J. Drug Deliv. Sci. Tec. 58 (2020) 101772 https://doi.org/10.1016/j.jddst.2020.101772.
[33] S. Joseph, H. Bunjes, Preparation of nanoemulsions and solid lipid nanoparticles by premix membrane emulsification, J. Pharm. Sci. 101 (2012) 2479–2489, https://doi.org/10.1002/jps.23163.
[34] R. Korać, D. Krajišnik, S. Savić, I. Pantelić, P. Iovančić, N. Cekić, J. Milić, A new class of emulsion systems – Fast inverted o/w emulsions: formulation approach, physical stability and colloidal structure, Colloids Surf. A 461 (2014) 267–278, https://doi.org/10.1016/j.colsurfa.2014.08.005.
[35] C. Belenki, M. Wilkenmann, M. Nieger, W. Gerlinger, B. Sachweh, H. P. Schuchmann, T. Muller, S. Bräse, Cleavable surfactants to tune the stability of W/O miniemulsions, J. Colloid Interface Sci. 393 (2013) 203–209, https://doi.org/10.1016/j.jcis.2012.10.072.
[36] M.L. Unbehauen, E. Fleige, F. Paulus, B. Schemmer, S. Mecking, S.D. Moré, R. Haag, Biodegradable core-multishell nanocarriers: Influence of inner shell structure on the encapsulation behavior of dexamethasone and tacrolimus, Polymers 9 (2017) 316, https://doi.org/10.3390/polym9080316.
[37] C.P. Tan, M. Nakajima, Effect of polyglycerol esters of fatty acids on physicochemical properties and stability of β-carotene nanodispersions prepared by emulsification/evaporation method, J. Sci. Food Agric. 85 (2005) 121–126, https://doi.org/10.1002/jsfa.1947.
[38] N. Duerr-Auster, T. Eisele, R. Wepf, R. Gunde, E.J. Windhab, Influence of pH on colloidal properties and surface activity of polyglycerol fatty acid ester vesicles, J. Colloid Interface Sci. 327 (2008) 446–450, https://doi.org/10.1016/j.jcis.2008.08.047.
[39] J. Li, C. Chang, W. Chen, Y. Su, L. Gu, Y. Yang, J. Zhai, Hybrid liposomes composed of hydrophilic emulsifiers and lecithin: Physicochemical, interaction and curcumin loading properties, Colloids Surf. A 655 (2022) 130210, https://doi.org/10.1016/j.colsurfa.2022.130210.
[40] M.M. Il'in, M.G. Semenova, L.E. Belyakova, A.S. Antipova, Y.N. Polikarpov, Thermodynamic and functional properties of legumin (11S globulin from *Vicia faba*) in the presence of small-molecule surfactants: Effect of temperature and pHY, J. Colloid Interface Sci. 278 (2004) 71–80, Doi: 10.1016/j.jcis.2004.05.039.
[41] C. Curschellas, J. Kohlbrecher, T. Geue, P. Fischer, B. Schmitt, M. Rouvet, E. J. Windhab, H.J. Limbach, Foams stabilized by multilamellar polyglycerol ester self-assemblies, Langmuir 29 (2013) 38–49, https://doi.org/10.1021/la3029116.
[42] N. Duerr-Auster, R. Gunde, R. Mäder, E.J. Windhab, Binary coalescence of gas bubbles in the presence of a non-ionic surfactant, J. Colloid Interface Sci. 333 (2009) 579–584, https://doi.org/10.1016/j.jcis.2009.01.016.
[43] C. Curschellas, R. Keller, R. Berger, U. Reitzler, D. Fell, H.-J. Butt, H.J. Limbach, Scanning force microscopy as a tool to investigate the properties of polyglycerol ester foams, J. Colloid Interface Sci. 374 (2012) 164–175, https://doi.org/10.1016/j.jcis.2012.01.031.
[44] P. Kubbutat, U. Kulozik, Interactions of sugar alcohol, di-saccharides and polysaccharides with polysorbate 80 as surfactant in the stabilization of foams, Colloids Surf. A 616 (2021) 126349, https://doi.org/10.1016/j.colsurfa.2021.126349.
[45] H. Kunieda, L.K. Shrestha, D.P. Acharya, H. Kato, Y. Takase, J.M. Gutiérrez, Super-stable nonaqueous foams in diglycerol fatty acid esters-non polar oil systems, J. Dispers. Sci. Technol. 28 (2007) 133–142, https://doi.org/10.1080/01932690600992779.
[46] G. Zhang, C. Bao, K. Fu, Y. Lin, T. Li, H. Yang, Synthesis, characterization, self-assembly, and irritation studies of Polyglyceryl-10 Caprylates, Polymers 12 (2020) 294, https://doi.org/10.3390/polym12020294.
[47] T. Kato, T. Nakamura, M. Yamashita, M. Kawaguchi, T. Kato, T. Itoch, Surfactant properties of purified polyglycerol monolaurates, J. Surfactants Deterg. 6 (2003) 331–337, https://doi.org/10.1007/s11743-003-0278-x.
[48] C. Curschellas, K. Nagy, E. Windhab, H.J. Limbach, Characteristics of polyglycerol ester and its different fractions, J. Colloid Interface Sci. 393 (2013) 182–191, https://doi.org/10.1016/j.jcis.2012.10.063.
[49] M.G. Semenova, L.E. Belyakova, A.S. Antipova, Yu.N. Polikarpov, L. Klouda, A. Markovic, M.M. Il'in, Effect of maltodextrins on the surface activity of small-molecule surfactants, Colloids Surf. B 31 (2003) 47–54, Doi: 10.1016/S0927-7765(03)00042-0.
[50] S. Ai, M. Ishitobi, Effects of the number of fatty acid residues on the phase behaviors of decaglycerol fatty acid esters, J. Colloid Interface Sci. 296 (2006) 685–689, https://doi.org/10.1016/j.jcis.2005.09.029.
[51] J.F. Ontiveros, C. Pierlot, M. Catté, V. Molinier, J.-L. Salager, J.-M. Aubry, Structure-interfacial properties relationship and quantification of the amphiphilicity of well-defined ionic and non-ionic surfactants using the PIT-slope method, J. Colloid Interface Sci. 448 (2015) 222–230, https://doi.org/10.1016/j.jcis.2015.02.028.
[52] N.C. Christov, K.D. Danov, P.A. Kralchevsky, K.P. Ananthapadmanabhan, A. Lips, Maximum bubble pressure method: Universal surface age and transport mechanisms in surfactant solutions, Langmuir 22 (2006) 7528–7542, https://doi.org/10.1021/la061239h.
[53] R.D. Stanimirova, K.G. Marinova, K.D. Danov, P.A. Kralchevsky, E.S. Basheva, S. D. Stoyanov, E.G. Pelan, Competitive adsorption of the protein hydrophobin and an ionic surfactant: parallel vs sequential adsorption and dilatational rheology, Colloids Surf. A 457 (2014) 307–317, https://doi.org/10.1016/j.colsurfa.2014.06.002.
[54] E.S. Basheva, P.A. Kralchevsky, K.D. Danov, K.P. Ananthapadmanabhan, A. Lips, The colloid structural forces as a tool for particle characterization and control of dispersion stability, Phys. Chem. Chem. Phys. 9 (2007) 5183–5198, https://doi.org/10.1039/B705758J.
[55] Y. Ao, C. Han, L. Kong, Y. Shen, S. Zhao, W. Liu, S. Zhou, Influence of different types of surfactants on the flotation of natural quartz by dodecylamine, Molecules 29 (2024) 2256, https://doi.org/10.3390/molecules29102256.
[56] P.A. Kralchevsky, K.D. Danov, V.L. Kolev, G. Broze, A. Mehreteab, Effect of nonionic admixtures on the adsorption of ionic surfactants at fluid interfaces. 1. Sodium dodecyl sulfate and dodecanol, Langmuir 19 (2003) 5004–5018, https://doi.org/10.1021/la0268496.
[57] K.D. Danov, R.D. Stanimirova, P.A. Kralchevsky, E.S. Basheva, V.I. Ivanova, J. T. Petkov, Sulfonated methyl esters of fatty acids in aqueous solutions: interfacial and micellar properties, J. Colloid Interface Sci. 457 (2015) 307–318, https://doi.org/10.1016/j.jcis.2015.07.020.
[58] C. Tanford, The Hydrophobic Effect: formation of Micelles and Biological Membranes, 2nd ed., Wiley, New York, 1980.
[59] P.A. Kralchevsky, K.D. Danov, C.I. Pishmanova, S.D. Kralchevska, N.C. Christov, K. P. Ananthapadmanabhan, A. Lips, Effect of the precipitation of neutral-soap, acid soap, and alkanoic acid crystallites on the bulk pH and surface tension of soap solutions, Langmuir 23 (2007) 3538–3553, https://doi.org/10.1021/la0625401.
[60] S.I. Karakashev, E.D. Manev, Hydrodynamics of thin liquid films: Retrospective and perspectives, Adv. Colloid Interface Sci. 222 (2015) 398–412, https://doi.org/10.1016/j.cis.2014.07.010.
[61] F. Mustan, N. Politova-Brinkova, Z. Vinarov, D. Rossetti, P. Rayment, S. Tcholakova, Interplay between bulk aggregates, surface properties and foam stability of nonionic surfactants, Adv. Colloid Interface Sci. 302 (2022) 102618, https://doi.org/10.1016/j.cis.2022.102618.